Mathematical Medicine and Biology (2014) **31**, 17–44
doi:10.1093/imammb/dqs029
Advance Access publication on December 4, 2012

Modelling fibrinolysis: a 3D stochastic multiscale model

Brittany E. Bannish*
Department of Mathematics and Statistics, University of Central Oklahoma, 100 North University Dr., Box 129, Edmond, OK 73034, USA
*Corresponding author: bbannish@uco.edu

and

James P. Keener and Aaron L. Fogelson
Departments of Mathematics and Bioengineering, University of Utah, 155 South 1400 East, Room 233, Salt Lake City, UT 84112-0090, USA

[Received on 8 September 2011; revised on 12 October 2012; accepted on 17 October 2012]

Fibrinolysis, the proteolytic degradation of the fibrin fibres that stabilize blood clots, is initiated when tissue-type plasminogen activator (tPA) activates plasminogen to plasmin, the main fibrinolytic enzyme. Many experiments have shown that coarse clots made of thick fibres lyse more quickly than fine clots made of thin fibres, despite the fact that individual thick fibres lyse more slowly than individual thin fibres. The generally accepted explanation for this is that a coarse clot with fewer fibres to transect will be degraded faster than a fine clot with a higher fibre density. Other experiments show the opposite result. The standard mathematical tool for investigating fibrinolysis has been deterministic reaction–diffusion models, but due to low tPA concentrations, stochastic models may be more appropriate. We develop a 3D stochastic multiscale model of fibrinolysis. A microscale model representing a fibre cross section and containing detailed biochemical reactions provides information about single fibre lysis times, the number of plasmin molecules that can be activated by a single tPA molecule and the length of time tPA stays bound to a given fibre cross section. Data from the microscale model are used in a macroscale model of the full fibrin clot, from which we obtain lysis front velocities and tPA distributions. We find that the fibre number impacts lysis speed, but so does the number of tPA molecules relative to the surface area of the clot exposed to those molecules. Depending on the values of these two quantities (tPA number and surface area), for given kinetic parameters, the model predicts coarse clots lyse faster or slower than fine clots, thus providing a possible explanation for the divergent experimental observations.

Keywords: fibrin; enzymatic degradation; lysis front; lysis speeds.

1. Introduction

Intravascular blood clots (thrombi) are composed of platelets, red blood cells and a stabilizing mesh of fibrin fibres. Fibrinolysis is the proteolytic degradation of fibrin fibres. Occlusive thrombi can form if fibrinolysis happens too slowly, causing heart attack or stroke. If fibrinolysis happens too quickly, however, blood clots may not form, leading to excessive bleeding. Understanding the tightly regulated fibrinolytic process is important from both physiological and clinical standpoints. Safely and effectively increasing lysis rates therapeutically is a goal of much ongoing research. When administered near a clot, a therapeutic bolus of tissue-type plasminogen activator (tPA) has been shown to increase the rate of fibrinolysis in patients. In several experiments mimicking therapeutic lysis, a bolus of tPA is added to the edge of a fibrin clot in the absence of fluid flow (Collet *et al.*, 2000; Sakharov *et al.*, 1996; Sakharov

& Rijken, 1995). These studies show that lysis moves across the clot as a front, with a high accumulation of lytic enzymes bound to fibres at the front.

The primary proteins involved in fibrinolysis are fibrin, plasmin, plasminogen (PLG) and tPA. Plasmin, the main fibrinolytic enzyme, exists in the blood plasma at extremely low concentration due to strong plasmin inhibitors. Consequently, plasmin must be created locally on the fibrin fibres. Plasmin is activated by tPA from its inactive precursor, PLG, after formation of a ternary complex of fibrin–tPA–PLG; when tPA and PLG are bound in close proximity on a fibre, tPA can activate PLG to plasmin. As plasmin degrades fibrin, initially cryptic tPA and PLG binding sites become exposed, creating a positive feedback for plasmin activation and fibrin degradation.

Plasmin-mediated degradation of fibrin fibres seems to occur by transverse cutting across fibres, rather than by uniform degradation around fibre diameters (Blinc *et al.*, 2000; Collet *et al.*, 2000; Veklich *et al.*, 1998). This is likely due to the fibre configuration, which has binding sites located 6 nm apart transversely and 22.5 nm apart lengthwise. It is hypothesized that plasmin can 'crawl' to the transverse binding sites, but is unable to reach farther away binding sites (Weisel *et al.*, 1999), which directs degradation across a fibre. A single fibre is a lateral aggregation of many two-stranded protofibrils, long chains composed of half-staggered 45-nm-long fibrin monomers. The protofibrils in a fibre are in register and clear striations across the fibre are seen in electron micrographs (Weisel, 1986). This half staggering distributes binding sites in 22.5 nm intervals along a fibre, while lateral aggregation spaces protofibrils 6 nm apart transversely.

Despite the seemingly tight packing of protofibrils into fibres, fibrin fibres contain about 20% protein and 80% water (Carr & Hermans, 1978; Voter *et al.*, 1986). Hence, on the scale of a single fibre, it is believed that there are pores through which small molecules can diffuse (Weisel & Litvinov, 2008). On the clot scale, there are much larger pores *between* fibres. The structure of a fibrin clot depends on the environment in which it forms. Conditions of high salinity or thrombin concentration result in fine clots with thin, tightly packed fibres (small pores), while conditions of low salinity or thrombin concentration produce coarser clots with thicker fibres and larger pores. Some experiments have shown that coarse clots made of thick fibres lyse more quickly than fine clots made of thin fibres (Carr & Alving, 1995; Collet *et al.*, 1993), despite the fact that individual thick fibres lyse more slowly than individual thin fibres (Collet *et al.*, 2000, 2003). However, other experiments show fine clots lyse faster than coarse clots or show no significant difference in lysis rates (Diamond & Anand, 1993; Kolev *et al.*, 1997; Wu *et al.*, 1994). We want to elucidate the factors that influence lysis speeds in clots of varying structure, in an effort to suggest targets for the design of new therapeutics aimed at breaking up blood clots. If plasmin cuts across fibres, a coarse clot with fewer fibres to transect will presumably be degraded faster than a fine clot with a higher fibre density. This explanation seems intuitive, however, it is difficult to confirm experimentally. In the current paper, we use a multiscale mathematical model of fibrinolysis to show that fibre number impacts lysis speed, but so does the number of tPA molecules relative to the surface area of the clot exposed to those molecules. Depending on the values of these two quantities (tPA number and surface area), coarse clots lyse faster or slower than fine clots.

Our microscale model of single fibre lysis is described in detail in Section 2.1 and our macroscale model of full clot lysis is described in Section 2.2. Results from both models are presented in Section 3 and implications of these results are discussed in Section 4.

2. The model

Previous models of fibrinolysis consist predominantly of 1D reaction, advection and diffusion equations (Anand *et al.*, 1995; Diamond & Anand, 1993; Wootton *et al.*, 2002; Zidanšek & Blinc, 1991).

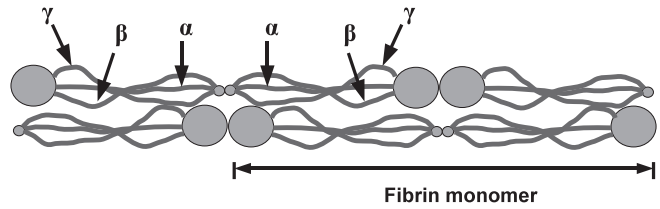

FIG. 1. Schematic of a two-stranded protofibril: a protofibril is a linear aggregation of fibrin monomers. Each fibrin monomer has two pairs of three chains, α, β and γ. Since a protofibril consists of two strands of half-staggered fibrin monomers, there are a total of 6 chains (two each of α, β and γ) that must be cut by plasmin to degrade the protofibril.

All of these models assume that initially fibrin is distributed homogeneously throughout the domain. In our companion paper (Bannish *et al.*, 2012), we included spatial heterogeneity in a deterministic 1D reaction–diffusion model, in an attempt study lysis of fine and coarse clots. We concluded that these types of models are insufficient, both qualitatively and quantitatively, to explore lysis speeds for varying clot structures. Here, we develop a 3D, stochastic multiscale model of fibrinolysis of a fibrin clot formed in plasma. Because tPA appears in such low concentration (70 pM in plasma (Weisel & Litvinov, 2008), but even the 5 nM concentration used in some experiments is only 3 molecules/μm^3 (Collet *et al.*, 2000)), a deterministic model (based on reaction–diffusion PDEs) is not appropriate; our stochastic model tracks individual tPA molecules rather than tPA concentrations. In contrast, the plasma concentration of PLG is 2 μM (Weisel & Litvinov, 2008). How the model tracks PLG, as well as plasmin and fibrin, is described in detail below. The microscale model represents an individual fibre cross section, while the macroscale model represents the full, 3D fibrin clot. Data collected from the microscale model are used in the macroscale model.

Experimental evidence suggests that fibres are cut transversely (Blinc *et al.*, 2000; Collet *et al.*, 2000; Veklich *et al.*, 1998), so we assume that lysis of a fibre can be approximated by the degradation of fibrin within a single cross section. Furthermore, we assume that the cross section is an arrangement of protofibril cross sections. Each strand of a two-stranded protofibril has three chains, α, β and γ (Fig. 1), which must be cleaved by plasmin, for a total of six chains requiring cutting (Weisel, 1986).

Terminology used in this section is as follows: a 'binding site' is a structure on fibrin to which one of the proteins tPA, PLG or plasmin can bind. A 'binding doublet' is a pair of adjacent binding sites. A 'binding location' is a physical region on a fibre where binding doublets are located. 'Exposed binding doublets' are doublets to which proteins can bind. 'Cryptic (or unexposed) binding doublets' are doublets that must be exposed by plasmin-mediated degradation before they are able to bind proteins. 'Available binding sites' refer to all the binding sites on the surface of a fibre, which we assume are the binding sites accessible to tPA.

2.1 *Microscale model*

Biochemical reactions that occur in a fibre cross section are considered in the microscale model. To simplify the numerics, the domain is a square of equal area to a circular fibre cross section. A thin cylindrical fibre with a diameter of 100 nm has cross sectional area $A = \pi(50\,\text{nm})^2 \approx (90\,\text{nm})^2$, so we use a square domain with side 90 nm. PLG and tPA binding sites are located 6 nm apart across a fibre (Weisel *et al.*, 1999), yielding 15 binding locations along a distance of 90 nm. This gives a total of 15^2 equally spaced binding locations within the square domain (Fig. 3c). A thick fibre (200 nm diameter) has 30^2 binding locations. Each binding location is a physical region containing a specified number

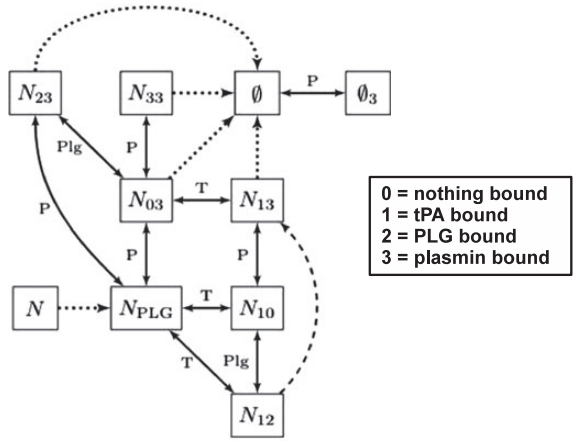

FIG. 2. Microscale model reaction diagram: the arrows show the possible reactions for each time step. Solid arrows indicate binding and unbinding of enzymes, with letters identifying which enzyme is involved (T is tPA, P is plasmin and Plg is plasminogen). Dashed arrow indicates activation of PLG to plasmin and dotted arrows indicate plasmin-mediated degradation of doublets or exposure of cryptic binding sites. A note on notation: N_{ij} is a doublet with species i and j bound, for i, j=0 (nothing), 1 (tPA), 2 (PLG) or 3 (plasmin). N is a cryptic doublet and N_{PLG} is a doublet with only PLG or nothing bound (N_{22}, N_{02}, or N_{00}). $\emptyset$ is a degraded doublet and $\emptyset_3$ is a degraded doublet with a bound plasmin molecule.

of binding doublets (Fig. 3d), which are pairs of binding sites to which tPA, PLG or plasmin can bind. Initially each binding location contains one exposed doublet, with five other cryptic doublets that can be exposed by plasmin-mediated cleavage. We think of a binding location as a cross section of a protofibril and that the six binding doublets represent the six protofibril chains.

Several different reactions are included in the microscale model (Fig. 2). The enzymes tPA, PLG and plasmin bind to, and unbind from, binding doublets distributed throughout the domain. When tPA and PLG are bound to the same doublet, tPA can activate PLG to plasmin. It is believed that PLG molecules are small enough to diffuse freely through pores in the fibre (Weisel & Litvinov, 2008), so we assume that PLG from the plasma phase can bind anywhere within a fibre cross section. We assume that the binding affinity of tPA to fibrin is so strong that tPA only binds to doublets on the fibre surface, even though it is capable of diffusing through the fibre (see Table 1 for parameter values). When PLG and tPA unbind from doublets, they return to the plasma phase. When plasmin unbinds, we imagine that it is preparing to crawl to a neighbouring binding site or binding location (i.e. within a protofibril or to a neighbouring protofibril), as proposed in Weisel *et al.* (1999), rather than entering the plasma phase. This protects the plasmin from strong plasma-phase inhibitors and consequently prevents the loss of plasmin molecules from the system. Plasmin crawling will be discussed in more detail in the following paragraph.

A binding doublet, which represents a portion of a fibrin monomer, can be degraded by a bound plasmin molecule. When a doublet is degraded, all proteins bound to it are immediately released and treated as if they had unbound. We assume that PLG and tPA are no longer able to bind to this degraded doublet. However, because we assume that plasmin is never entirely unbound, but rather crawls to neighbouring doublets in the cross section, we allow plasmin to move anywhere in the domain, regardless of whether or not the doublets are degraded. We imagine plasmin cuts a ‘groove’ in the fibre, with frayed ends of protofibrils on either end of the groove. By assuming that there are always frayed ends of fibre to which plasmin can crawl, we allow plasmin to occupy a doublet that has been degraded, but do not allow it

to degrade that doublet any further. However, bound plasmin can expose initially cryptic doublets at whatever binding location it occupies, even if it is bound to a degraded doublet. We assume that only one plasmin molecule can be bound to a particular degraded doublet.

Our simulation of the lytic process begins with one tPA molecule placed randomly on the surface of the fibre (the first row of the computational domain, Fig. 3c). Because tPA is found at low concentrations, we consider only cross sections with a single tPA molecule. We apply the Gillespie algorithm (Gillespie, 1976, 1977) to find the event times for the various microscale reactions depicted in Fig. 2. The Gillespie algorithm gives a statistically exact realization of the process described by the master equation

$$\frac{\partial P}{\partial t}(\underline{x}, t|\underline{x}_0, t_0) = \sum_{j=1}^{22}[a_j(\underline{x} - \underline{v}_j)P(\underline{x} - \underline{v}_j, t|\underline{x}_0, t_0) - a_j(\underline{x})P(\underline{x}, t|\underline{x}_0, t_0)].$$

Here, $P(\underline{x}, t|\underline{x}_0, t_0)$ is the probability that the system is in state $\underline{x}$ at time t having been in state $\underline{x}_0$ at time t_0. Given the current state $\underline{x}$ at time t and the set of possible reactions and reaction rates as described by the stoichiometric vectors $\underline{v}_j$ and propensity function $\underline{a}$, the Gillespie algorithm makes provisional choices of the length of time after t that each possible reaction will happen. (See Appendix for details about the Gillespie algorithm, $\underline{x}$, $\underline{v}_j$, $\underline{a}$.) The next time step (and associated event) is chosen to be the minimum of the Gillespie provisional reaction times.

We explicitly model only the doublets that contain tPA or plasmin. Empty doublets and doublets with only PLG bound are grouped into one state called N_{PLG} (see Fig. 2 caption for explanation of notation). Assuming that PLG binding is in quasi-steady state gives us probabilities of PLG being on doublets. We do not model individual PLG molecules. The dissociation constant for PLG binding to fibrin changes depending on whether fibrin is intact or 'nicked' (partially degraded): $k_D^{\mathrm{intact}} = 38\,\mu\mathrm{M}$, $k_D^{\mathrm{nicked}} = 2.2\,\mu\mathrm{M}$ (Lucas *et al.*, 1983; Sakharov & Rijken, 1995). In the model, any doublet that was cryptic initially and became exposed is considered to be on nicked fibrin. The probability of a nicked or intact N_{PLG} being in state N_{00}, N_{02} or N_{22} is calculated using the quasi-steady state assumption for PLG (see Appendix).

When a reaction releases the tPA molecule (either by unbinding or degradation of the doublet to which it was bound), we calculate the probability of the molecule rebinding to the same cross section, rather than diffusing away. If the tPA rebinds, we assume that it binds to an available binding site on a doublet at most two binding locations away from where it unbound. If the molecule does not rebind, we assume that it has diffused away from the cross section and is removed from the system, and that no more plasmin can be produced. We calculated the rebinding probability by solving a 3D escape problem as described in the Appendix, and found that for the situation and parameters of relevance here, tPA essentially never rebinds.

We define lysis to be complete (i.e. the fibre to be cleaved) when a specific fraction (typically 2/3) of the total number of binding doublets (exposed plus unexposed) have been degraded by plasmin. We assume that fibres are under tension (Liu *et al.*, 2010), hence fibres snap after a percentage of binding doublets are degraded. Our assumption that both thin and thick fibres lyse when 2/3 of the doublets are degraded is reasonable if we assume that thick fibres are under four times as much tension as thin fibres. We present an intuitive justification for this assumption. Imagine that we pull on a fine and on a coarse clot (described in the following section) with a fixed force in a fixed direction. The cross-sectional areas of the two clots are the same, but there are different numbers of fibres in each area. In fact, there are about four times as many thin fibres in a given area as there are thick. So, if the same load is distributed among the given fibres, a single thick fibre must bear four times the load of a single thin fibre.

In summary, the microscale model is written algorithmically as follows.

(1) Initialize the system, set t_{final} (a prescribed final time) and randomly place one tPA molecule on the first row of binding locations.

(2) Determine whether the tPA-containing doublet is N_{10} or N_{12} using the quasi-steady state approximation for PLG.

(3) While $t < t_{\text{final}}$,

  (a) apply Gillespie algorithm to each doublet containing a tPA or plasmin molecule to determine the next reaction event and associated time;

  (b) assign the smallest time from step (a) as the next time step. Update t and use the corresponding event to update the system;

    (i) if the event results in the unbinding of tPA, calculate the rebinding probability to determine whether tPA rebinds or is removed. For our parameters, tPA is always removed;

    (ii) if the event results in the unbinding (i.e. crawling) of plasmin, randomly assign plasmin to an available binding site on a neighbouring binding location (it is allowed to stay on its current binding location) and update the state of the new doublet;

  (c) calculate the percentage of degraded doublets:

    (i) if degradation $<2/3$, return to step (a);

    (ii) if degradation $\geqslant 2/3$, stop the algorithm because lysis is complete;

(4) If $t \geqslant t_{\text{final}}$, algorithm terminates and lysis fails.

From the microscale model, we save the time tPA unbound from the cross section (the tPA leaving time), the number of plasmin molecules that were created and the time at which lysis completed (the lysis time). We use this information from hundreds of microscale model simulations to create distributions that we use in the macroscale model.

2.2 *Macroscale model*

Data generated from the microscale model are used in a macroscale model of clot lysis. We make the simplifying assumption that the clot is a 3D square lattice (rather than a tangled mesh of fibres), with each lattice edge representing one fibre. Pore size, defined as the distance between fibres, is the length of one fibre. To mimic experiments, the clot is assumed to be contained in a small chamber with volume $V = \text{depth} \times \text{width} \times \text{height}$ (Fig. 3a). We assume that the width and height of the chamber are equal and that the depth of the chamber is of the same order of magnitude. Rather than model the full 3D system, we consider a periodic slice of clot, with depth equal to a single pore size. We think of this slice as running between edge midpoints, so the 1-fibre depth is actually composed of two halves of two separate fibres. To obtain the lattice dimensions, we fix the fibrin concentration per fibre at 824 μM (Carr & Hermans, 1978; Voter *et al.*, 1986), the fibrin concentration in the clot at

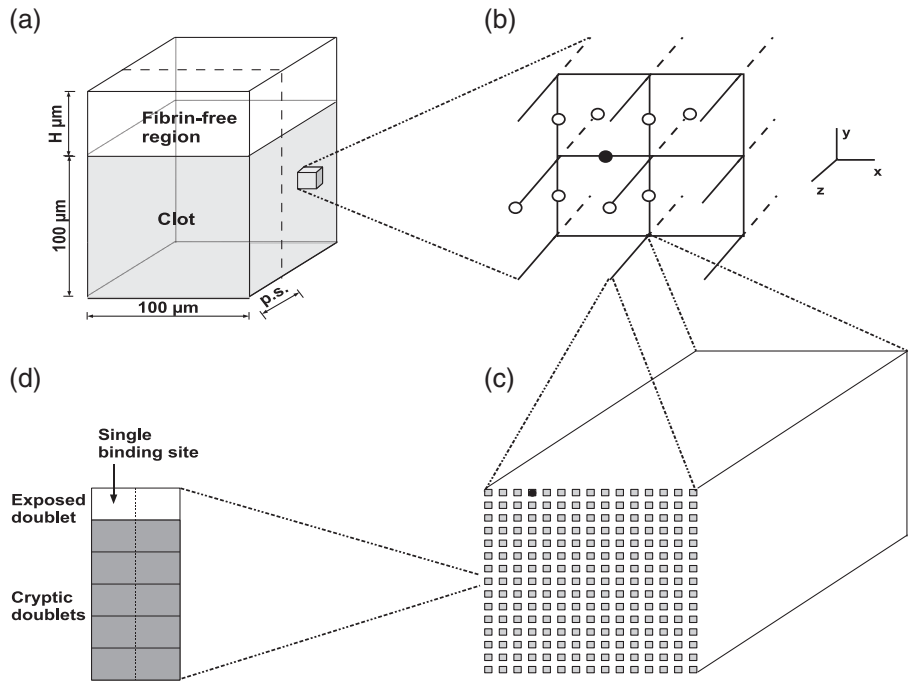

FIG. 3. (a) Diagram of macroscale clot: the clot is formed in a chamber with a fibrin-free region in which tPA is added. When we simulate the model, we only consider a 100-μm × 100-μm × p.s. (pore size) periodic slab of the clot, denoted by the dashed line. We consider fibrin-free regions of different sizes, so H (height of fibrin-free region) varies. (b) Macroscale diffusion of tPA on a lattice: white circles indicate the fibres that the tPA molecule (black circle) can reach in one time step. The tPA molecule can diffuse to the four neighbouring edges in the plane of the page, diffuse out of the page to the two neighbouring solid edges (which each represent half of a fibre extending out of the plane), or diffuse into the page to the two neighbouring dotted edges (which represent half of the fibres extending into the plane). Boundary conditions are periodic in the z-direction and reflecting in the other two dimensions. (c) Microscale domain for thin fibre: this is a 90 nm × 90 nm square domain with 225 binding locations (grey squares) spaced 6 nm apart (not drawn to scale). One tPA molecule (black dot) is randomly placed on a doublet in the first row of the domain, which represents the fibre surface. (d) One binding location: each binding location initially contains one exposed doublet (white boxes) and five unexposed doublets (grey boxes). A binding doublet is composed of two binding sites.

8.8 μM (Diamond & Anand, 1993) and the height and width of the chamber at 100 μm (to assure the system is big enough to avoid boundary effects). Then using the radii of the fibres, we calculate the pore size and the number of fibres required to keep the concentrations at their fixed values. This results in a fine clot with 13,333 fibres and pore size 1.42 μm and a coarse clot with 3,400 fibres and pore size 2.84 μm. N, the number of nodes in one row of the lattice, is thus equal to 67 for a fine clot and 34 for a coarse clot.

A fibrin-free space of height H extends above the clot chamber (Fig. 3a). We fill this fibrin-free volume with a tPA solution to mimic a therapeutic bolus of tPA administered at the edge of a clot (this also mimics many *in vitro* experiments). We prescribe the initial tPA concentration in the fibrin-free space and we can vary the bolus size by changing H. The tPA molecules are uniformly distributed on ghost lattice edges in this fibrin-free volume. These edges are arranged in the same square lattice formation as the clot, but they do not contain fibrin and hence cannot be degraded.

Since our aim is to compare macroscale lysis velocities between two different clots, it is necessary to use the same total fibrin concentration in both fine and coarse clots and to use the same relative amount of tPA to initiate lysis. We imagine that the coarse and fine clots are formed in the same size chamber, so their volumes are equal. Since we only model a periodic slab of each clot, of depth equal to pore size, and because the pore size is twice as big in the coarse clot, the volume of clot (as well as the volume of the fibrin-free region) is also twice as big. Therefore, we put twice as many tPA molecules in the fibrin-free region abutting the coarse clot as we do in the fine clot. This assures that the total tPA concentration averaged over the fibrin-free volume is conserved.

Detailed biochemistry was considered in the microscale model, so the macroscale model includes only tPA binding, unbinding and diffusion, as well as degradation of fibres. When a tPA molecule binds to a fibre, it initiates the lytic cascade on the microscale. The molecule is assigned a leaving time using the microscale model leaving time distribution. When the current time is greater than or equal to the leaving time, the tPA molecule unbinds. Using microscale data, the tPA leaving time determines the number of plasmin molecules that will be created in that particular cross section. The number of plasmin molecules determines the time it will take the fibre to be cut (see Fig. 6). In this way, every edge to which tPA binds has an associated degradation time. When the current time is greater than or equal to an edge's degradation time, the edge is degraded and any tPA still bound to it is released.

During each fixed time step, we allow tPA to bind or unbind and any unbound tPA to move by diffusion to a neighbouring fibre. The tPA in the fibrin-free region can only diffuse, as there is no fibrin to which it may bind. Reflecting boundary conditions are imposed on the four sides of the clot adjacent to the walls of the microchamber and periodic boundary conditions are imposed in the small third dimension since we consider a periodic slab of clot.

The size of the fixed time step used in the macroscale model is the typical time needed for one molecule to diffuse to one of the eight neighbouring edges. In the simulations, we associate every tPA molecule with a particular edge so that all the macroscale events happen on the lattice edges. By associating each tPA molecule with one edge, we approximate the 3D diffusion problem by having tPA hop on the lattice (Fig. 3b). In this approximation, we think of an unbound molecule associated with an edge as being anywhere within a small distance of that edge, not necessarily directly on the fibre. A bound tPA molecule is bound directly to the edge on which it resides, but we do not model the exact location of tPA on a fibre, only which fibre tPA occupies. For simplicity in deriving the macroscale diffusion rules, we assume that molecules associated with a particular edge are located at the fibre midpoint (white circles in Fig. 3b). When multiple tPA molecules are bound to the same fibre, we assume that they are bound to different binding sites along the length of the entire fibre (and therefore capable of starting lysis in different cross sections), but for the purpose of diffusion we still consider them to be at fibre midpoints. The degradation time for an edge with multiple bound tPA molecules is the minimum of the times obtained for each molecule. Since tPA can still diffuse in the whole domain regardless of degradation status of edges, tPA molecules may be associated with degraded edges, but cannot bind to them.

To derive the time it takes a molecule to diffuse to a neighbouring fibre, consider a tPA molecule on one of the horizontal edges (Fig. 3b). A neighbouring edge is defined as one of the eight closest edges, as measured diagonally from the edge midpoint. So, the neighbouring edges of a fibre oriented in the x-direction will be oriented in the y- and z-directions, since these are closer, diagonally, than any other x-direction edges. Let $P^n_{i,j,k}$ be the probability of a tPA molecule being at edge i, j, k at time n. Let q be

the probability of its moving to a neighbouring edge. Then,

$$\begin{aligned} P^{n+1}_{i,j,k} &= (1-q)P^n_{i,j,k} + \frac{q}{8}\Big\{P^n_{i-1,j+1,k} + P^n_{i+1,j+1,k} + P^n_{i+1,j-1,k} + P^n_{i-1,j-1,k} \\ &\quad + P^n_{i-1,j,k+1} + P^n_{i+1,j,k+1} + P^n_{i+1,j,k-1} + P^n_{i-1,j,k-1}\Big\} \\ \Longrightarrow \Delta t\frac{\partial P}{\partial t} &\approx \frac{q}{8}\{P(x-\Delta x, y+\Delta y, z) + P(x+\Delta x, y+\Delta y, z) + P(x+\Delta x, y-\Delta y, z) \\ &\quad + P(x-\Delta x, y-\Delta y, z) + P(x-\Delta x, y, z+\Delta z) + P(x+\Delta x, y, z+\Delta z) \\ &\quad + P(x+\Delta x, y, z-\Delta z) + P(x-\Delta x, y, z-\Delta z) - 8P(x,y,z)\}. \end{aligned}$$

Expanding the right-hand side gives

$$\Delta t\frac{\partial P}{\partial t} = \frac{q}{8}\left(4\Delta x^2\frac{\partial^2 P}{\partial x^2} + 2\Delta y^2\frac{\partial^2 P}{\partial y^2} + 2\Delta z^2\frac{\partial^2 P}{\partial z^2}\right), \tag{2.1}$$

where $\Delta x = \Delta y = \Delta z = \frac{1}{2}$(pore size). Doing this derivation for a molecule on an edge in the y-direction results in the equation

$$\Delta t\frac{\partial P}{\partial t} = \frac{q}{8}\left(2\Delta x^2\frac{\partial^2 P}{\partial x^2} + 4\Delta y^2\frac{\partial^2 P}{\partial y^2} + 2\Delta z^2\frac{\partial^2 P}{\partial z^2}\right), \tag{2.2}$$

while the derivation for a molecule on an edge in the z-direction results in the equation

$$\Delta t\frac{\partial P}{\partial t} = \frac{q}{8}\left(2\Delta x^2\frac{\partial^2 P}{\partial x^2} + 2\Delta y^2\frac{\partial^2 P}{\partial y^2} + 4\Delta z^2\frac{\partial^2 P}{\partial z^2}\right). \tag{2.3}$$

Recall that if a tPA molecule moves, it *must* move onto an edge oriented in one of the other two directions. So, there is biased movement away from fibres oriented in the same direction as the fibre with tPA. But because this is true for fibres oriented in all three principal directions, the overall diffusion is given by the average of Equations (2.1–2.3). This gives

$$\frac{\partial P}{\partial t} = D\nabla^2 P,$$

where $D = (q/12\Delta t)(\text{pore size})^2$ is the diffusion coefficient for tPA. Rearranging gives the macroscale time step:

$$\frac{\Delta t}{q} = \frac{(\text{pore size})^2}{12D}. \tag{2.4}$$

We do not explicitly know q, the probability of a molecule moving to a neighbouring edge, but it does not matter since the ratio $\Delta t/q$ is fixed. As long as we choose a q that makes Δt small enough that our method converges, the actual choice of q does not matter. For the macro results presented in this paper, we use $q = 0.2$, $D = 5 \times 10^{-7}$ cm^2/s so $\Delta t \approx 6.72 \times 10^{-4}$ s for a fine clot and 2.69×10^{-3} s for a coarse clot.

Every time a tPA molecule unbinds or diffuses to a new edge, we use an exponential distribution to choose the time at which the molecule will bind to the edge:

$$t_{\text{bind}} = t - \frac{\ln(\hat{r}_1)}{k_{\text{on}}^{\text{tPA}} b} - \frac{\Delta t}{2},$$

where t is the current time, $\hat{r}_1$ is a random variable uniformly distributed on [0,1] ($\hat{r}_1 \in U[0,1]$), $k_{\text{on}}^{\text{tPA}}$ is the binding rate of tPA to fibrin and b is the concentration of available tPA binding sites. We bind a molecule at time t (a multiple of Δt) if $t_{\text{bind}} \leqslant t$. The subtraction of a half time step, $\Delta t/2$, in the definition of t_{bind} eliminates bias in the algorithm and implies that binding actually occurs at the time t closest to t_{bind}. For the same reason, we also subtract $\Delta t/2$ from the degradation and unbinding times selected from the microscale model distributions.

The macroscale model is expressed algorithmically as follows.

(1) Determine the clot geometry and Δt, set $t = 0$, fix t_{final} (a prescribed final time) and initialize the degradation times of all edges to 0.

(2) Randomly place a specified number of tPA molecules in the fibrin-free region.

(3) For $t \leqslant t_{\text{final}}$:

  (a) set $t = t + \Delta t$;

  (b) degrade any edges with nonzero degradation times $\leqslant t$ and unbind any tPA molecules that were bound to the degraded edges;

  (c) check the unbinding times for all bound tPA molecules, unbind any with times $\leqslant t$;

  (d) assign each newly unbound molecule a binding time, t_{bind};

  (e) for each unbound molecule, pick a random number $\hat{r} \in U[0,1]$;

    (i) if $\hat{r} \leqslant (1-q)$, the molecule does not move;

      (A) if $t_{\text{bind}} > t$ or the edge has already been degraded, the tPA remains unbound;

      (B) if $t_{\text{bind}} \leqslant t$ and the edge the molecule is on has not been degraded, bind the molecule and use the microscale distributions to find the new unbinding time, the number of plasmin molecules produced, and the degradation time for that fibre;

    (ii) if $\hat{r} > (1-q)$, the molecule has the opportunity to move, but may bind before it can do so;

      (A) if $t_{\text{bind}} > t$ or the edge has already been degraded, randomly move the tPA to a neighbouring edge and calculate a new binding time for the tPA to that edge;

      (B) if $t_{\text{bind}} \leqslant t$ and the edge the molecule is on has not been degraded, pick a random number, $\hat{r}_2 \in U[0,1]$;

(I) if $\hat{r}_2 > (t - t_{\text{bind}})/\Delta t$, then movement happens before the tPA binds. Randomly move the tPA to a neighbouring edge and calculate a new binding time for the tPA to that edge;

(II) if $\hat{r}_2 \leqslant (t - t_{\text{bind}})/\Delta t$, the molecule binds and therefore cannot move. Use the micro model distributions to calculate a new unbinding time, the number of plasmin molecules produced, and the degradation time for the fibre;

(f) return to step (a).

3. Results

3.1 *Microscale model results*

To explore the range of model behaviour (and because not all parameter values have been measured), we use four different parameter sets, shown in Table 1. Since this is a stochastic model, we report the statistics of many independent simulations. The microscale model results presented in this section are given as median (first quartile Q1, third quartile Q3) of 600 simulations and the macroscale model results are mean $\pm$ standard deviation of 10 simulations. In some instances of the microscale simulation, lysis of an individual fibre did not occur because tPA unbound before creating any plasmin. These failed runs are excluded from single fibre lysis time data since they would yield an infinite lysis time; the microscale results presented are therefore the average lysis times conditional upon successful lysis.

3.1.1 *tPA leaving time.* From the microscale model we obtain distributions of the tPA leaving time (the time at which tPA diffuses away from the cross section), the number of plasmin molecules produced, and the single fibre lysis time for thin and thick fibres for all parameter sets (Table 2). As expected, the thick fibre takes longer to degrade. Unexpectedly, for Case A and B parameters, tPA stays bound to the thick fibre slightly longer than it stays bound to the thin fibre, even though the same tPA binding and unbinding rates are used. The tPA unbinding rate in Cases A and B is small enough that tPA rarely unbinds. Instead, tPA is released from the fibre when plasmin degrades the doublet to which it is bound. For plasmin to force the release of tPA, the two molecules must be sharing a doublet when a plasmin-mediated degradation event is chosen by the Gillespie algorithm. With the given parameter values, plasmin molecules can crawl many times between degradation events. Thick fibres have more doublets that the plasmin molecules can crawl to, so plasmin shares a doublet with tPA less frequently in thick fibres than in thin; this is responsible for the increased tPA residence time on thick fibres. With Case C and D parameters, the tPA unbinding rate is larger than in Cases A and B, and tPA almost always unbinds before it encounters plasmin. The tPA leaving times in thin and thick fibres are very similar in these cases since the dynamics are dominated by the tPA kinetic rates, which do not depend on fibre size.

3.1.2 *Effect of the definition of degradation and of the degradation rate on single fibre lysis.* Since there are four times as many binding doublets in a thick fibre as a thin fibre, it would be reasonable to expect that a thick fibre would take four times as long to degrade. The model results support this hypothesis (Fig. 4). Because we do not know the exact percentage of doublets that must be degraded

TABLE 1 *Parameter sets used in the model: Case A is the baseline parameter set and Cases B, C, D differ from Case A only in their starred entries. The tPA binding and unbinding rates are changed in Cases C and D, but the dissociation constant ($k^D_{tPA} = k^{off}_{tPA}/k^{on}_{tPA}$) remains fixed. The dissociation constant for PLG is different depending on whether fibrin is intact or nicked and the dissociation constant for tPA is different depending on whether tPA is bound to a doublet with PLG or without PLG. k^{on}_i and k^{off}_i are the binding rate of species i to fibrin and the unbinding rate of species i from fibrin, respectively, for i = tPA, PLG or plasmin (PLi). k^{ap}_{cat} is the catalytic rate constant for activation of PLG to plasmin (PLi), k^n_{cat} is the catalytic rate constant for plasmin-mediated exposure of cryptic binding doublets and k_{deg} is the plasmin-mediated rate of fibrin degradation. We know the dissociation constants for tPA and PLG, but not the individual rates, so references in the table are for k_D.*

Parameters	Case A	Case B	Case C	Case D	Reference
k_{deg} (s^{-1})	10	1*	10	1*	
k^{off}_{PLG} (s^{-1})	3.8	3.8	3.8	3.8	*,⋆
k^{on}_{PLG}, intact ($\mu M^{-1}\,s^{-1}$)	0.1	0.1	0.1	0.1	*
k^{on}_{PLG}, nicked ($\mu M^{-1}\,s^{-1}$)	1.7273	1.7273	1.7273	1.7273	⋆
k^{off}_{PLi} (s^{-1})	38	38	38	38	§
k^{off}_{tPA}, with PLG (s^{-1})	0.0002	0.0002	0.02*	0.02*	†
k^{off}_{tPA}, without PLG (s^{-1})	0.0036	0.0036	0.36*	0.36*	‡
k^{on}_{tPA} ($\mu M^{-1}\,s^{-1}$)	0.01	0.01	1.0*	1.0*	†,‡
k^{ap}_{cat} (s^{-1})	50	50	50	50	
k^n_{cat} (s^{-1})	10	1*	10	1*	

*Lucas *et al.* (1983); ⋆Sakharov & Rijken (1995); § Kolev *et al.* (1997), estimated; †Bachmann (1994); ‡Horrevoets *et al.* (1994).

TABLE 2 *Microscale model results: entries are median (Q1, Q3) of 600 independent simulations, except for lysis time, which is the result of only those simulations that produced a plasmin molecule. The column labeled 'Runs with PLi' gives the number of runs, out of 600, that resulted in production of plasmin.*

Parameters	Fibre diameter (nm)	tPA leaving time (s)	Number of plasmin molecules	Lysis time (min)	Runs with PLi
Case A	100	7.98 (3.26, 14.90)	2 (1, 3)	1.59 (1.12, 2.73)	587
	200	8.46 (3.34, 16.80)	2 (1, 3)	5.98 (4.06, 11.05)	594
Case B	100	37.60 (19.40, 69.39)	7 (4, 13)	3.19 (2.30, 5.61)	589
	200	42.35 (17.79, 73.64)	7 (4, 14)	11.38 (6.99, 21.53)	586
Case C	100	1.60 (0.64, 3.13)	0 (0, 1)†	2.64 (2.47, 2.77)	701*
	200	1.63 (0.66, 3.19)	0 (0, 1)†	10.93 (10.29, 11.45)	713*
Case D	100	1.94 (0.77, 3.87)	0 (0, 1)†	20.87 (10.88, 21.53)	732*
	200	1.90 (0.85, 3.92)	0 (0, 1)†	84.15 (42.82, 85.75)	690*

†Q1 and the median are both 0 because the majority of the runs generated no plasmin.
*To generate enough lysis time data, 1800 runs were used instead of 600.

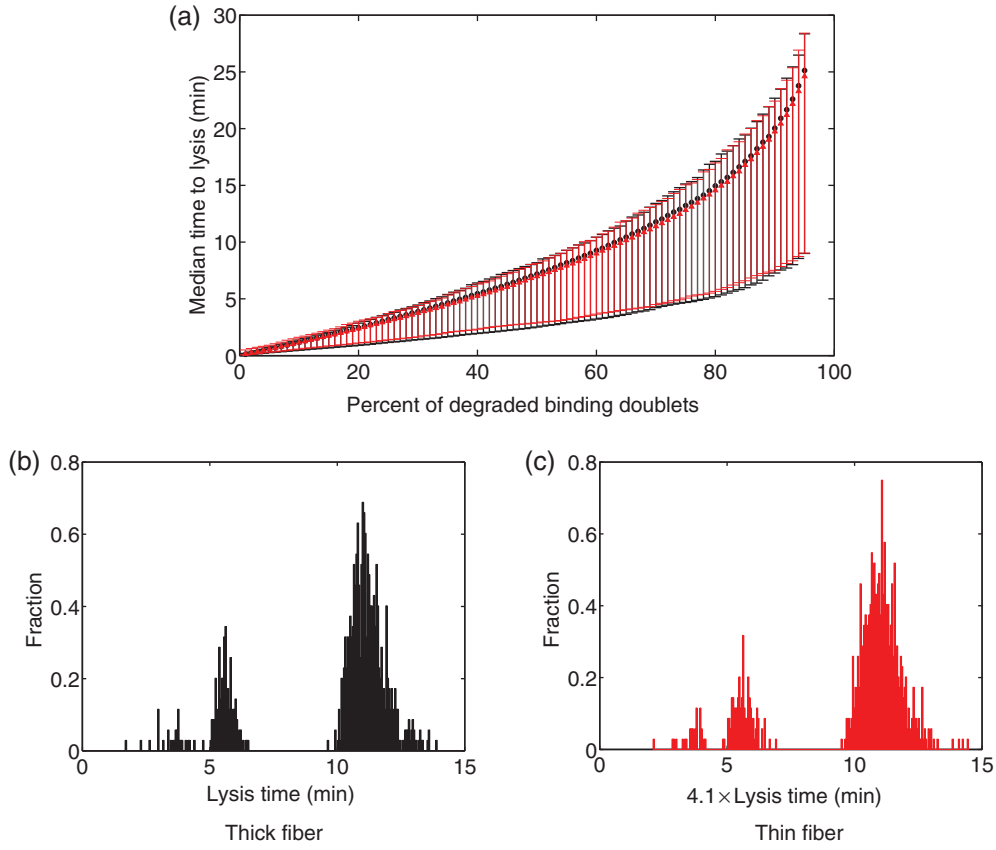

FIG. 4. Single fibre lysis time data for Case C parameters. (a) Single fibre lysis times as a function of the percentage of binding doublets that must be degraded for lysis to be complete: black circles denote median lysis time, top error bar (black) represents the 95th percentile and bottom error bar (black) represents the 5th percentile, for a thick fibre. Triangles (red online) denote 4 × (median lysis time), with top and bottom error bars (red online, gray in print) 4 × (95th percentile), respectively, for a thin fibre; thick fibre lysis times are ∼4 times longer than thin fibre lysis times. (b), (c) Normalized single fibre lysis time distributions for a thick fibre and a thin fibre, respectively, with lysis defined as degradation of 2/3 of the total number of doublets. The thin fibre lysis times are scaled by a factor of 4.1, showing that the range of the thick fibre lysis time distribution is ∼4 times larger than the range of the thin fibre lysis time distribution. The distributions have several peaks because the lysis times directly correlate to the number of plasmin molecules produced, which is discrete. For example, the large, right-most peak corresponds to runs when only one plasmin molecule was created.

before the fibre can be considered lysed, we vary our definition of lysis from 1% of total doublets degraded to 95% of total doublets degraded and see how median lysis times are affected. As Fig. 4(a) shows, thin fibres lyse four times faster than thick fibres, on average, regardless of how we define lysis. Normalized single fibre lysis time distributions for Case C parameters are shown in Fig. 4(b,c), for lysis defined as degradation of 2/3 of the total doublets. The thick and thin single fibre lysis time distributions look very similar when the thin fibre lysis times are multiplied by a factor of 4.1. This is close to the factor of four that relates the medians of the data, as seen in Fig. 4(a).

Insight into how the degradation rate k_{deg} affects lysis is gained by comparing Case A with Case B. With baseline parameter values (Case A), plasmin attempts to degrade a doublet 10 times per second,

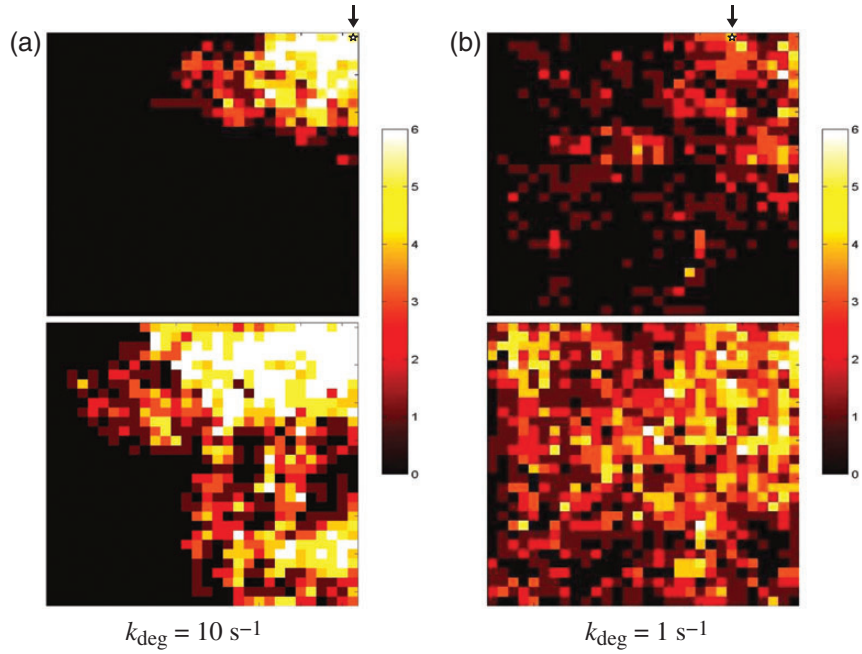

FIG. 5. Fibrin degradation in a cross section of a 200 nm diameter fibre: each pixel represents a binding location that contains six doublets. The colour bar indicates level of degradation, with lighter colours denoting higher levels of degradation. The pixel ranges from black if none of the doublets at a particular binding location have been degraded, to white if all six binding doublets have been degraded. Top images show cross sections with one-tenth of binding doublets degraded and bottom images are cross sections with one-third of binding doublets degraded. The arrows point to a white star in the top images, which indicates the location of tPA. (a) Case A parameters: with $k_{deg} = 10\,s^{-1}$, lysis is localized because plasmin is not able to move very far between degradation events. Top image at $t = 33.91$ s, bottom image at $t = 72.42$ s. (b) Case B parameters: with $k_{deg} = 1\,s^{-1}$, lysis happens throughout the cross section because plasmin can move a considerable distance between degradation events. Top image at $t = 84.74$ s, bottom image at $t = 188.82$ s.

on average. In the case with low degradation rate (Case B), plasmin does this once per second. For thick fibres, 3.5 times more plasmin is produced in Case B than in Case A on average (7 vs. 2 molecules, respectively). While it seems reasonable that more plasmin would result in faster lysis, lysis times are actually about 1.9 times longer with lower degradation rates because the plasmin is less efficient (11.38 min for Case B vs. 5.98 min for Case A). A similar result is seen for thin fibres. If plasmin only degrades once per second, ~10 times more plasmin is needed to get the same lysis time as Case A. Clearly lysis depends on plasmin efficiency, not solely on the number of plasmin molecules produced.

The degradation rate, k_{deg}, affects not only the lysis time, but also the pattern of lysis. With a higher degradation rate, lysis is localized and moves like a wave through the cross section (Fig. 5(a)). Plasmin molecules are created on the doublet with tPA and they cannot move very far between degradation events. Therefore, plasmin degrades the area around the tPA doublet first. The plasmin molecules slowly move away from the tPA doublet, systematically spreading lysis as they go. Contrast this with Case B, where $k_{deg} = 1\,s^{-1}$. Here, plasmin can crawl a considerable distance between degradation events and start lysis in many locations throughout the cross section (Fig. 5(b)). Further investigation is required to determine whether the pattern of microscale lysis is important or if the single fibre lysis time alone is important for macroscale degradation.

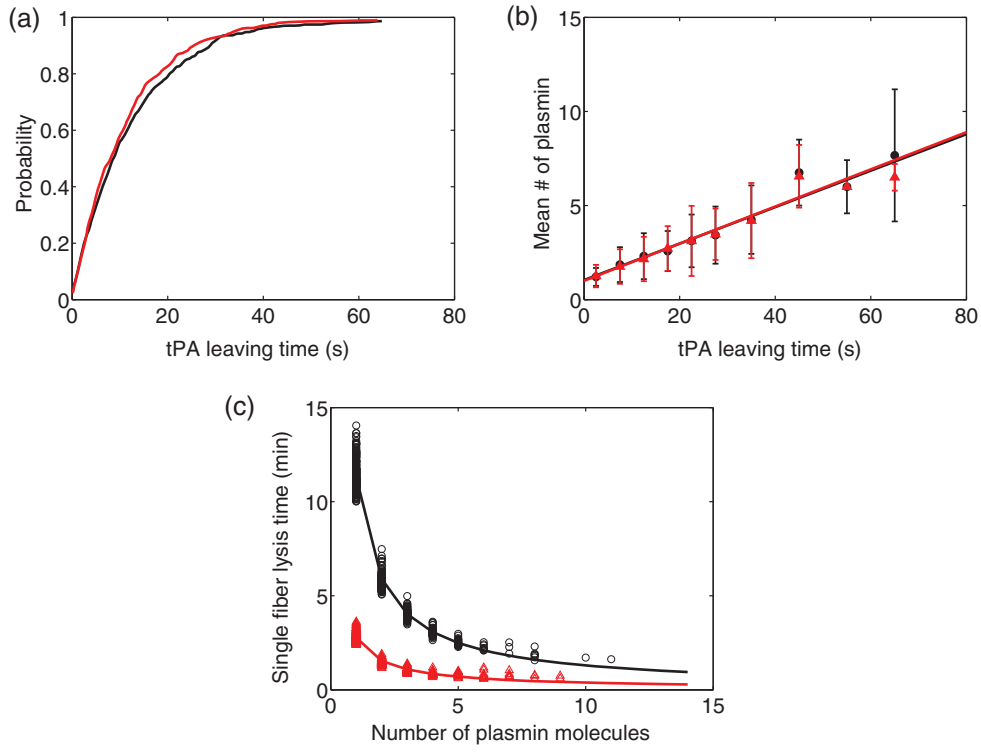

FIG. 6. Microscale model results for 100 nm fibre (red online, gray in print) and for 200 nm fibre (black) with Case A parameters: triangles (red online) indicate thin fibre data, black circles indicate thick fibre data. (a) Empirical cumulative distribution function of tPA leaving times. (b) The best fit lines of the data relating tPA leaving time to the number of plasmin molecules produced. The raw data are binned in 5 s intervals from 0 to 30 s (e.g. 0–5 s, 5–10 s, etc.) and 10 s intervals from 30 s onward. Means of each bin are plotted at the interval midpoint. A line is then fit to the means, weighted by the number of data points in each bin. (c) The best fit curves of the data relating number of plasmin to single fibre lysis time.

3.1.3 *Microscale model data used in macroscale model.* The microscale data are incorporated into the macroscale model as follows. Running 600 independent simulations of the microscale model with each fibre diameter, 100 and 200 nm, generates the data in Fig. 6. First, we obtain an empirical cumulative distribution function for tPA leaving times (Fig. 6(a)). This distribution is used in the macroscale model to randomly pick a tPA leaving time every time a tPA molecule binds to a fibre. Next, we bin the number of plasmin molecules produced into tPA leaving time intervals. For tPA leaving times ranging from 0 to 30 s, we create 5-s intervals in which to bin the plasmin data. For tPA leaving times greater than 30 s, we create 10-s intervals in which to bin the plasmin data. We find the mean of the data in each bin and fit a line to these means, weighted by the number of data points in each bin (Fig. 6b). In the macroscale model, we use this line to determine the number of plasmin molecules produced for a given tPA leaving time. Unsurprisingly, more plasmin is produced for larger tPA leaving times. Finally, we fit a power function to the scatter plot of lysis time versus plasmin number data and use it to determine the lysis time (Fig. 6c). As expected, lysis times are long when only a few plasmin molecules are created and shorter when there is more plasmin. The data displayed in Fig. 6 are all the microscale model information needed for the macroscale model.

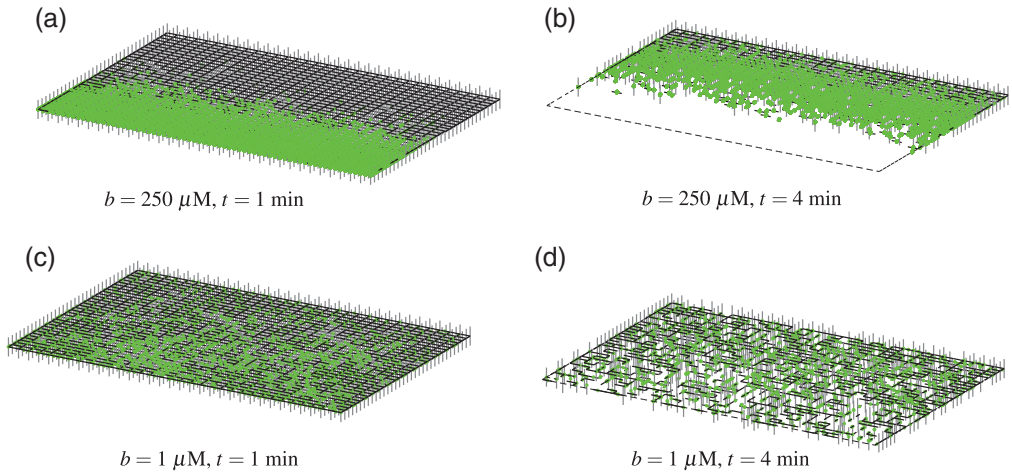

FIG. 7. The 3D distribution of tPA and state of degradation for a coarse clot with Case A parameters: ∼44,200 tPA molecules (a 5 nM concentration) were randomly distributed in the $51.68 \times 100 \times 3.04\,\mu\text{m}^3$ fibrin-free region abutting the clot. Light (green online) asterisks denote bound tPA; unbound tPA is not plotted. Black segments represent fibrin fibres. The dashed lines in (b) and (d) indicate the border of the initial clot. The physical distance between lattice nodes is 3.04 μm. (a,b) State of the clot ∼1 and 4 min, respectively, after the introduction of tPA. The tPA binding site concentration per fibre is $b = 250\,\mu$M. (c,d) State of the clot ∼1 and 4 min, respectively, after the introduction of tPA. The tPA binding site concentration per fibre is $b = 1\,\mu$M.

3.2 *Macroscale model results*

3.2.1 *Qualitative observations.* Depending on the tPA binding site concentration per fibre, macroscale lysis can proceed as a front with a high accumulation of tPA molecules at the front (Fig. 7a,b) or lysis can occur throughout the clot in no particular pattern (Fig. 7c,d). We imagine that tPA binding sites are distributed throughout the fibrin fibres, but only those binding sites on the surface of the fibre are available to tPA as it diffuses through the clot. The thick fibres have half as many available binding sites per unit volume as the thin fibres. The argument is as follows. The binding site concentration, b, we use to calculate macroscale binding of tPA is the number of available binding sites per volume, which is the number of fibres per volume times the available binding sites per fibre. The former scales like $1/r^3$ and the latter is proportional to surface area per fibre and so scales like r^2.

Because the radius of our thick fibre is twice the radius of our thin fibre, $b_{\text{coarse}} = \frac{1}{2} b_{\text{fine}}$. The average length of time it takes for a tPA molecule to bind to a fibre is $(k_{\text{on}}^{\text{tPA}} b)^{-1}$. So, for a given binding rate, $k_{\text{on}}^{\text{tPA}}$, the time to bind is shorter for a higher b. A long tPA binding time means that the molecule can diffuse farther between binding events, effectively distributing the tPA more evenly throughout the clot. If tPA binds to fibres located throughout the clot, then it also initiates lysis on fibres located throughout the clot. Macroscale lysis in this case is not front-like (Fig. 7c,d). On the other hand, a short binding time means that the molecule is not able to diffuse very far between binding events, effectively localizing tPA at the clot front. In this case, lysis proceeds as a front (Fig. 7a,b).

3.2.2 *Lysis front velocity and degradation rate.* Besides the qualitative conclusions drawn above, we also obtain quantitative results about macroscale lysis. We use two different measures of macroscale lysis: front velocity and degradation rate. We measure front velocity of a given column of the lattice by tracking in time the y-position (same axes as Fig. 3b) of the first edge oriented in the y-direction that contains fibrin. This gives position versus time data from which we can estimate a front velocity. We do

TABLE 3 *Macroscale model results for Case A parameters with a tPA concentration of 5 nM: entries are mean ± standard deviation of 10 independent simulations. Front velocity calculations do not make sense for simulations in which lysis was not front-like, hence the 'n/a' in some entries.*

Clot type	b (μM)	H (μm)	Front velocity (μm/min)	Degradation rate (% fibres $\times 10^{-1}$/s)
Fine	2	51.68	n/a	4.29 ± 0.083
Coarse	1	51.68	n/a	4.11 ± 0.101
Fine	500	51.68	18.39 ± 0.47	3.03 ± 0.017
Coarse	250	51.68	16.83 ± 1.00	2.64 ± 0.048
Fine	500	3.04	10.02 ± 0.43	1.69 ± 0.015
Coarse	250	3.04	10.76 ± 0.90	1.75 ± 0.025

this for each of the columns extending above the N nodes on the bottom row of the lattice. So, we have N front velocities, which we average to obtain the overall lysis front velocity for the given simulation. We also calculate the standard deviation. We do 10 independent simulations, so the results presented in Table 3 are means of the 10 means ± means of the 10 standard deviations. Front velocity calculations begin when the first fibre degrades, not when the bolus of tPA is added to the fibrin-free region. We could instead have tracked how the position of fibres oriented in the z- or x-direction changes in time, but results would not be significantly different.

Degradation rate is a useful measure of lysis speed when the pattern of lysis is not front-like. To calculate the degradation rate, we plot the percentage of fibres degraded as a function of time. Lysis begins sometime after the addition of tPA and lysis of the last few fibres takes a bit longer, but the plot is linear in the middle range of times from shortly after lysis begins to shortly before lysis ends. Fitting a line to the linear part of this plot allows us to estimate a (percent degraded)/s degradation rate. We identify the linear part of the plot as the region between the first and last times that the slope between consecutive data points is $\geqslant 1 \times 10^{-3}$ (% degraded)/s. This eliminates the slowly changing initial and final data from the degradation rate calculation. Because we do 10 independent simulations, the results presented in Table 3 are means of the 10 independent degradation rates ± the standard deviation of the 10 degradation rates.

The macroscale lysis results presented in Table 3 are for Case A parameters with a bolus of 5 nM tPA solution added to the fibrin-free region. The volume of 5 nM solution added varies, since we change the height of the fibrin-free region in some of the simulations. For a fibrin-free region that is approximately half the height of the clot, 51.68 μm, lysis is not front-like and fine clots lyse faster than coarse (as measured by degradation rate) when $b = 2$ μM for the fine clot and 1 μM for the coarse clot. When $b = 500$, 250 μM for fine and coarse clots, respectively, lysis proceeds as a front and fine clots lyse faster than coarse clots. However, if we keep the larger binding site concentrations and simply change the height of the fibrin-free region to 3.04 μm (i.e. change the volume of tPA solution we add), then lysis is still front-like, but coarse clots lyse faster than fine.

3.2.3 *Effect of tPA on lysis front velocity.* It is not simply the number of fibres that determines which type of clot lyses faster; the number of tPA molecules in the system relative to the surface area of the clot abutting the fibrin-free region has a strong influence on lysis speeds. Figure 8 shows fine and coarse front velocities as a function of this tPA-to-surface-area ratio for Case A parameters. Several different tPA concentrations and fibrin-free volumes were used, but these values on their own do not

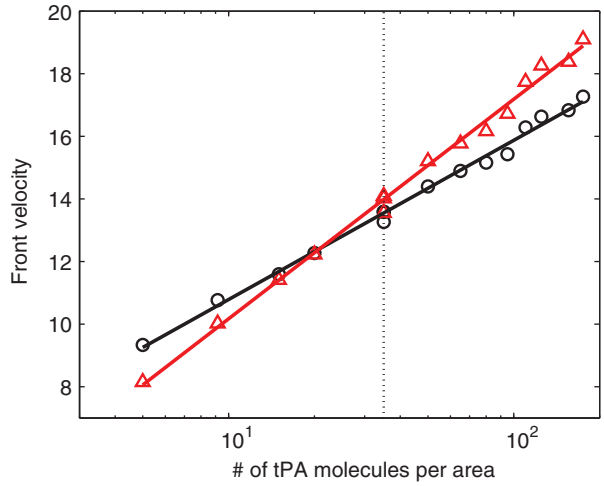

FIG. 8. Lysis front velocity for fine clot (triangles, red online) and coarse clot (black circles) as functions of the ratio of number of tPA molecules to surface area of clot exposed to the fibrin-free region: symbols are means of 10 runs. Dashed line indicates three runs with fixed tPA-to-surface-area ratio. Velocities are measured in μm/min. Fifteen different experiments were run with tPA-to-surface-area ratios varying from 5 to 175 molecules/μm^2 and corresponding front velocities were calculated.

matter; it is the total number of tPA molecules relative to the surface area (which we fix at 100 μm × pore size) that affects lysis rate. As the tPA-to-surface-area ratio increases, so does the front velocity. Since we keep the surface area of the clot fixed, we can only increase the ratio by increasing the number of tPA molecules in the system. The way we do so, however, does not matter, as long as the fibrin-free region is not too big. We can keep the size of the fibrin-free region fixed and use a larger tPA concentration or we can fix the tPA concentration and increase the size of the fibrin-free region. Both methods increase the number of tPA molecules used in the simulation. The dotted line in Fig. 8 represents this. We ran three different simulations of the macroscale model using the same number of tPA molecules, but three different fibrin-free volumes and tPA concentrations. For a fine clot, the two upper triangles are almost indistinguishable—they look like one triangle. For these two runs, we used tPA concentrations of 19.12 and 6.37 nM and fibrin-free heights of 3.04 and 9.12 μm, respectively. This shows that the same tPA-to-surface-area ratio produces the same front velocity, as long as the fibrin-free region is not too big. When we took a fibrin-free height of 51.68 μm and a 1.12 nM tPA concentration (the lower triangle), we got a slightly slower front velocity, even though the ratio was the same as in the other two simulations. This is because there is so much fibrin-free space into which the tPA molecules can diffuse, that they encounter the clot, and consequently begin lysis, less frequently.

The coarse front velocities respond similarly to the tPA-to-surface-area ratio (Fig. 8). By fitting a line to the data for both coarse and fine front velocities and calculating the point at which the two lines intersect, we estimate 25.09 molecules/μm^2 to be the tPA-to-surface-area ratio below which coarse clots lyse faster than fine. As the tPA-to-surface-area ratio increases, so does the fine-to-coarse front velocity ratio. With a fixed surface area, this means that as the number of tPA molecules increases, so does the fine front velocity relative to the coarse. This makes sense, because if the system were to contain enough tPA to bind to all the fibres at the front of the fine clot, the disadvantage of having more fibres would be erased. Lysis would be started on all the fibres at the lysis front, and since individual thin fibres lyse faster than thick fibres, the fine clot would degrade more quickly. On the other hand, if there are

sufficiently few tPA molecules, then lysis could not begin on all thin fibres at once. In this case, coarse clots would have the advantage of containing fewer fibres. There would be more tPA molecules per fibre in the coarse clots *and* there would be fewer fibres. Lysis would begin on a higher percentage of thick fibres than thin and, if that percentage were sufficiently high, this would cause the coarse clot to lyse faster than the fine one.

4. Discussion

In this paper, we have described a model of fibrinolysis that includes several new and important features: multiple dimensions, multiple scales and stochasticity. Detailed treatment of the biochemistry of lysis occurs in a microscale model of a single fibre cross section. Treatment of the overall clot lysis, including transport of the lysis-initiating enzyme tPA, occurs in a macroscale model which uses data obtained from microscale model simulations. We have shown that our 3D, stochastic model exhibits behaviour that is qualitatively consistent with the literature. Lysis proceeds as a front, with a high accumulation of tPA at the front. Individual thin fibres lyse more quickly than individual thick fibres and under certain conditions coarse clots composed of thick fibres lyse more quickly than fine clots composed of thin fibres. The faster degradation of coarse clots is based on the number of tPA molecules relative to the surface area of the clot and the fact that in a given clot volume there are fewer fibres to cut. When the tPA-to-surface-area ratio is small enough (for our parameters and clot geometries, <25.09 molecules/μm^2), there is not enough tPA to start lysis on all the thin fibres at the front of the fine clot. However, there *is* enough tPA to start lysis on all the thick fibres at the front of the coarse clot because there are fewer fibres. Despite the longer single fibre lysis times, coarse clots made of thick fibres lyse faster than fine clots in these situations because lysis must be started fewer times. However, for the same parameters and clot structures, if there is enough tPA at the clot edge to bind to all the thin fibres at the front of the fine clot, fine clots lyse faster than coarse. So, it is not simply fibre number that determines relative front velocities, but rather fibre number in conjunction with the number of tPA molecules exposed to the clot. For any tPA concentration, if the height of the fibrin-free region is small enough, then almost all the tPA molecules bind to fibres at the clot front within the first minute. Hence, the number of tPA molecules added to the system, and not the tPA concentration, matters. The overall lysis time is determined by the combination of individual fibre lysis time, the number of fibres in the clot needing to be cut and the number of tPA molecules per unit surface area of the clot front (which influences how many individual fibre lysis processes occur concurrently).

Rigorous comparisons of our multiscale model with published quantitative data remain a challenge. Comparing our results to experiments, we appear to get reasonable single fibre lysis times. The lysis times for our baseline parameters (Case A) are on the same order as experimentally observed times: the model predicts thin fibres lyse in 1.59 min and thick fibres lyse in 5.98 min, while (Collet *et al.*, 2000) measure thin fibres to lyse in 3.1 ± 1.1 minutes, and thick fibres to lyse in 5.4 ± 1.4 min. The definition of single fibre lysis in Collet *et al.*'s (2000) experiment is unclear, however. Presumably the fibre is considered lysed when it is no longer visible by the confocal microscope, but this is obviously different than our definition in which the fibre is lysed when it is cut by plasmin-mediated degradation of fibrin within a cross section. Further, it is not clear when the experimental clock starts to run because it is not possible to see when a tPA molecule binds to a fibrin fibre. More similar to the criterion in our model, Blinc *et al.* (2000) use atomic force microscopy (AFM) to obtain single fibre transection times of 7.6 ± 3.7 and 6.4 ± 4.2 min for thin and thick fibres, respectively, which according to the authors do not differ significantly. A fibre that was continuous in the previous AFM image but laterally split in the current image is considered lysed, but a single image takes 2–8 min to acquire: so, time resolution is

a serious issue. Additional data are necessary to verify our single fibre lysis results, but our numbers appear to be in a reasonable range.

The predicted lysis front velocities in fine and coarse clots are not as different as the measured rates. Collet *et al.* (2000) find coarse clots lyse at a rate of 31 μm/min and fine clots lyse at a rate of 2.15 μm/min. The fastest coarse front velocity we obtain is 17.27 μm/min, the slowest fine front velocity is 8.15 μm/min and the largest coarse-to-fine front velocity ratio is about 1.15. Wootton *et al.* (2002) measure lysis speeds ranging from 8.4 to 18.6 μm/min, under various flow conditions (which we do not include in the model), but do not distinguish between clot structures. In a different experiment, where 10 nM urokinase (a PLG activator that unlike tPA can activate unbound PLG) was added to the edge of a fibrin clot formed in buffer, the fine front velocity was about 12 μm/min while the coarse front velocity was about 25 μm/min (Wu *et al.*, 1994). If PLG is not pre-equilibrated with a fibrin clot, and instead is first introduced to the clot with the bolus of tPA (tPA 69.4 nM, PLG 2.4 μM), lysis speed is slower: 2.92 ± 0.57 μm/min for an unspecified clot structure (Dunn *et al.*, 2006). Not only are all these experiments (with the exception of Collet *et al.*, 2000) different than the situation we model, it also is unclear how the experimental front velocities are measured, which makes comparisons to our model difficult. We measure front velocities from the time the first fibre degrades, but measurements could also be taken from the time tPA is first introduced into the system or from some arbitrary time after lysis begins. Due to the wide range of lysis rates measured experimentally, it will be beneficial to have additional data with which to compare our model.

In a recent study, Longstaff *et al.* (2011) showed that when tPA variant delF-tPA (a tPA mutant lacking the finger domain) was added to the edge of a clot, after an initial transient front of lysis with localized delF-tPA, delF-tPA diffused ahead of the front and was distributed throughout a larger region of the clot. Lysis rates, estimated from changes in clot turbidity, were slower for lysis initiated by delF-tPA than by normal tPA. By lowering the concentration of available tPA binding sites in our model, we can eliminate the accumulation of tPA at the clot edge and the resulting front-like pattern of lysis. However, unlike Longstaff *et al.* (2011), distribution of tPA throughout the clot yields significantly faster lysis than tPA localized at the front. This suggests that therapeutics should be aimed at preventing tPA from accumulating at the lysis front. However, dispersal of tPA throughout the clot should be accomplished by minimal change to tPA structure, as Longstaff *et al.* (2011) showed that a tPA variant missing a key binding domain results in slower lysis.

The microscale model is able to predict the efficiency of individual molecules—something that is currently unattainable experimentally, since single molecules cannot be counted. Figure 6 illustrates how many plasmin molecules can be produced by a single tPA molecule and how the number of plasmin molecules determines lysis time. The microscale model predicts that for small tPA unbinding rates, a tPA molecule stays bound to a thick fibre slightly longer than it does to a thin fibre because plasmin is slower to encounter and degrade the doublet with tPA. We are not aware of any single-molecule experiments addressing this phenomenon (or if the experiments are even possible with current technology); this is an example of how mathematical models can be used to propose new avenues of research for laboratory scientists. Our prediction is a product of the assumptions that we made about microscale degradation and movement of plasmin (i.e. that tPA is released when plasmin degrades the fibrin to which tPA is bound and that plasmin crawls to neighbouring binding sites inside a fibre); an experiment to measure the length of time tPA stays bound to fibres of varying thickness would be worthwhile. If tPA stays bound to thick fibres longer, our model provides a hypothesis for why; if tPA does not stay bound to thick fibres longer, this suggests that either the physiological rate of tPA unbinding is large (Case C, D) or that one or more of our model assumptions needs modification. For instance, perhaps tPA remains bound to the fibre, even after the doublet has been degraded. Either way, we obtain useful information by comparing the model with experiments.

We find that the degradation rate affects both the time and pattern of single fibre lysis. Lower degradation rates produce slower lysis times and lead to degradation occurring throughout the cross section. Higher degradation rates result in faster lysis that moves as a wave across the fibre cross section.

Macroscale model results depend on single fibre lysis times, but we do not know what the lysis criteria for a single fibre should be. We assume that the fibre is cut when 2/3 of the binding doublets in a cross section are degraded. We justify this assumption with a plausible argument about fibres under tension. However, we could also have defined lysis to occur when a given number of doublets remain. If a fibre is cut when all but 100 binding doublets are degraded, lysis of the thick fibre will take longer, relative to lysis of the thin fibre, because the thick fibre has four times as many binding doublets. Even if lysis is dependent on percentage of doublets degraded rather than number, macroscale front velocities differ for varying values of this percentage. As Fig. 4a shows, single fibre lysis times increase nonlinearly as the percentage of doublets required for lysis increases from 1 to 95%. Choosing a percentage other than 66.67% changes the magnitude of the thin and thick lysis times, but the thin-to-thick lysis time ratio remains unchanged. Until there is more evidence for a 'correct' criterion for single fibre lysis, we believe our assumption is reasonable.

Analysis of our model results suggests several possible experiments. The hypothesis that the number of tPA molecules relative to the surface area of the clot exposed to those molecules determines which clot structure lyses faster should be testable in the lab. Also, current technology is such that individual fibrin fibres can be isolated and observed at shorter time intervals, meaning that more accurate single fibre lysis experiments should now be possible. The prediction of the model is that a thick fibre with diameter twice the thin fibre diameter will take four times longer to degrade. If the thick fibre experimental degradation time is longer than four times the thin fibre degradation time, this could suggest that the criteria for complete lysis are not that a certain *percentage* of doublets are lysed, but rather that a given *total number* of doublets remains, below which lysis is almost certain to occur. On the other hand, if the thick fibre lysis time is less than four times the thin fibre lysis time, this suggests that the unbinding of tPA by plasmin has a significant effect; tPA could be forced to unbind by plasmin-mediated degradation less frequently in thick fibres because of the additional space for plasmin to crawl. If tPA stays bound longer to a thick fibre than a thin fibre, more plasmin can be produced and lysis can happen faster than expected. As explained above, an experiment that tests the length of time tPA stays bound to fibres of various diameters would be interesting, but we are unsure if this type of experiment is currently feasible. Finally, our modelling suggests that a potential target for new therapeutics should be a tPA variant that has much of the same structure as tPA, but binds less strongly to the clot front. Understanding conditions which increase the lysis rates of clots of varying structure is important for improved blood clot therapies. The broad question of how to safely increase lysis rates clinically is ongoing motivation for our work. Our multiscale model is one step towards a better understanding of what influences fibrinolysis rates. Laboratory experiments to test our hypotheses will provide even more insight and direct future modelling efforts.

Acknowledgements

The authors would like to thank John Weisel for meaningful discussions. This work was supported by NSF grants DMS-0540779, RTG DMS-0354259, VIGRE DMS-0602219 and NIGMS grant R01-GM090203.

References

Anand, S., Wu, J. & Diamond, S. L. (1995) Enzyme-mediated proteolysis of fibrous biopolymers: dissolution front movement in fibrin or collagen under conditions of diffusive or convective transport. *Biotechnol. Bioeng.*, **48**, 89–107.

Bachmann, F. (1994) The plasminogen-plasmin enzyme system. *Hemostasis and Thrombosis: Basic Principles and Clinical Practice*, 3rd edn, chapter 84 (R. W. Colman *et al.*, eds). Philadelphia: J.B. Lippincott Company, pp. 1592–1622.

Bannish, B. E., Keener, J. P., Woodbury, M., Weisel, J. W. & Fogelson, A. L. (2012) Modelling fibrinolysis: 1-dimensional continuum models. *Math. Med. Biol.*, **31**, 45–64.

Blinc, A., Magdic, J., Fric, J.& Musevic, I. (2000) Atomic force microscopy of fibrin networks and plasma clots during fibrinolysis. *Fibrinolysis Proteol.*, **14**, 288–299.

Carr, M. & Alving, B. (1995) Effect of fibrin structure on plasmin-mediated dissolution of plasma clots. *Blood Coagul. Fibrin.*, **6**, 567–573.

Carr, M. & Hermans, J. (1978) Size and density of fibrin fibers from turbidity. *Macromolecules*, **11**, 46–50.

Collet, J. P., Lesty, C., Montalescot, G. & Weisel, J. W. (2003) Dynamic changes of fibrin architecture during fibrin formation and intrinsic fibrinolysis of fibrin-rich clots. *J. Biol. Chem.*, **278**, 21331–21335.

Collet, J. P., Park, D., Lesty, C., Soria, J., Soria, C., Montalescot, G. & Weisel, J. W. (2000) Influence of fibrin network conformation and fibrin fiber diameter on fibrinolysis speed: dynamic and structural approaches by confocal microscopy. *Arterioscler Thromb. Vasc. Biol.*, **20**, 1354–1361.

Collet, J. P., Soria, J., Mirshahi, M., Hirsch, M., Dagonnet, F., Caen, J. & Soria, C. (1993) Dusart syndrome: a new concept of the relationship between fibrin clot architecture and fibrin clot degradability: hypofibrinolysis related to an abnormal clot structure. *Blood*, **82**, 2462–2469.

Diamond, S. L. & Anand, S. (1993) Inner clot diffusion and permeation during fibrinolysis. *Biophys. J.*, **65**, 2622–2643.

Dunn, E. J., Philippou, H., Ariens, R. A. S. & Grant, P. J. (2006) Molecular mechanisms involved in the resistance of fibrin to clot lysis by plasmin in subjects with type 2 diabetes mellitus. *Diabetologia*, **49**, 1071–1080.

Gillespie, D. T. (1976) A general method for numerically simulating the stochastic time evolution of coupled chemical reactions. *J. Comput. Phys.*, **22**, 403–434.

Gillespie, D. T. (1977) Exact stochastic simulation of coupled chemical reactions. *J. Phys. Chem.*, **81**, 2340–2361.

Horrevoets, A. J. G., Smilde, A., de Vries, C. & Pannekoek, H. (1994) The specific role of finger and kringle 2 domains of tissue-type plasminogen activator during *in vitro* fibrinolysis. *J. Biol. Chem.*, **269**, 12639–12644.

Kolev, K., Tenekedjiev, K., Komorowicz, E. & Machovich, R. (1997) Functional evalutaion of the structural features of proteases and their substrate in fibrin surface degradation. *J. Biol. Chem.*, **272**, 13666–13675.

Liu, W., Carlisle, C., Sparks, E.& Guthold, M. (2010) The mechanical properties of single fibrin fibers. *J. Thromb. Haemostasis*, **8**, 1030–1036.

Longstaff, C., Thelwell, C., Williams, S. C., Silva, M. M. C. G., Szabó, L. & Kolev, K. (2011) The interplay between tissue plasminogen activator domains and fibrin structures in the regulation of fibrinolysis: kinetic and microscopic studies. *Blood*, **117**, 661–668.

Lucas, M. A., Fretto, L. J. & McKee, P. A. (1983) The binding of human plasminogen to fibrin and fibrinogen. *J. Biol. Chem.*, **258**, 4249–4256.

Sakharov, D. V., Nagelkerke, J. F. & Rijken, D. C. (1996) Rearrangements of the fibrin network and spatial distribution of fibrinolytic components during plasma clot lysis. *J. Biol. Chem.*, **271**, 2133–2138.

Sakharov, D. V. & Rijken, D. C. (1995) Superficial accumulation of plasminogen during plasma clot lysis. *Circulation*, **92**, 1883–1890.

Veklich, Y., Francis, C. W., White, J.& Weisel, J. W. (1998) Structural studies of fibrinolysis by electron microscopy. *Blood*, **92**, 4721–4729.

Voter, W. A., Lucaveche, C. & Erickson, H. P. (1986) Concentration of protein in fibrin fibers and fibrinogen polymers determined by refractive index matching. *Biopolymers*, **25**, 2375–2384.

Weisel, J. W. (1986) Fibrin assembly: lateral aggregation and the role of the two pairs of fibrinopeptides. *Biophys. J.*, **50**, 1079–1093.

Weisel, J. W. & Litvinov, R. I. (2008) The biochemical and physical process of fibrinolysis and effects of clot structure and stability on the lysis rate. *Cardiovas. Hematol. Agents Med. Chem. (Formerly Current Medicinal Chemistry—Cardiovascular & Hematological Agents)*, **6**, 161–180(20).

Weisel, J. W., Veklich, Y., Collet, J. P. & Francis, C. W. (1999) Structural studies of fibrinolysis by electron and light microscopy. *Thromb. Haemostasis*, **82**, 277–282.

Wootton, D. M., Popel, A. S. & Alevriadou, B. R. (2002) An experimental and theoretical study on the dissolution of mural fibrin clots by tissue-type plasminogen activator. *Biotechnol. Bioeng.*, **77**, 405–419.

Wu, J. H., Siddiqui, K. & Diamond, S. L. (1994) Transport phenomena and clot dissolving therapy: an experimental investigation of diffusion-controlled and permeation-enhanced fibrinolysis. *Thromb. Haemostasis*, **72**, 105–112.

Zidanšek, A. & Blinc, A. (1991) The influence of transport parameters and enzyme kinetics of the fibrinolytic system on thrombosis: mathematical modelling of two idealised cases. *Thromb. Haemostasis*, **65**, 553–559.

A. Appendix

A.1 *Detailed definitions for Gillespie algorithm*

Here, we define the specific vectors that appear in the master equation,

$$\frac{\partial P}{\partial t}(\underline{x}, t|\underline{x}_0, t_0) = \sum_{j=1}^{22}[a_j(\underline{x} - \underline{\nu}_j)P(\underline{x} - \underline{\nu}_j, t|\underline{x}_0, t_0) - a_j(\underline{x})P(\underline{x}, t|\underline{x}_0, t_0)],$$

that describes the microscale model reactions. Using the notation explained in Fig. 2, the state vector is

$$\underline{x} = [N_{\mathrm{PLG}}, \quad N_{12}, \quad N_{10}, \quad N_{13}, \quad N_{03}, \quad N_{23}, \quad N_{33}, \quad \emptyset, \quad \emptyset_3, \quad N], \tag{A.1}$$

where x_i is the number of molecules of type i in the system. The stoichiometric matrix describing the 22 possible reactions that can occur is

$$\underline{\nu} = \begin{pmatrix} \underline{\nu}_1 \\ \underline{\nu}_2 \\ \underline{\nu}_3 \\ \underline{\nu}_4 \\ \underline{\nu}_5 \\ \underline{\nu}_6 \\ \underline{\nu}_7 \\ \underline{\nu}_8 \\ \underline{\nu}_9 \\ \underline{\nu}_{10} \\ \underline{\nu}_{11} \\ \underline{\nu}_{12} \\ \underline{\nu}_{13} \\ \underline{\nu}_{14} \\ \underline{\nu}_{15} \\ \underline{\nu}_{16} \\ \underline{\nu}_{17} \\ \underline{\nu}_{18} \\ \underline{\nu}_{19} \\ \underline{\nu}_{20} \\ \underline{\nu}_{21} \\ \underline{\nu}_{22} \end{pmatrix} = \begin{pmatrix} 0 & -1 & 1 & 0 & 0 & 0 & 0 & 0 & 0 & 0 \\ 0 & 1 & -1 & 0 & 0 & 0 & 0 & 0 & 0 & 0 \\ 0 & 0 & 1 & -1 & 0 & 0 & 0 & 0 & 0 & 0 \\ 0 & 0 & 0 & -1 & 1 & 0 & 0 & 0 & 0 & 0 \\ 0 & 0 & 0 & 0 & -1 & 1 & 0 & 0 & 0 & 0 \\ 0 & 0 & 0 & 0 & 1 & -1 & 0 & 0 & 0 & 0 \\ 0 & 0 & 0 & 0 & 1 & 0 & -1 & 0 & 0 & 0 \\ 1 & -1 & 0 & 0 & 0 & 0 & 0 & 0 & 0 & 0 \\ 1 & 0 & -1 & 0 & 0 & 0 & 0 & 0 & 0 & 0 \\ 1 & 0 & 0 & 0 & -1 & 0 & 0 & 0 & 0 & 0 \\ 1 & 0 & 0 & 0 & 0 & -1 & 0 & 0 & 0 & 0 \\ 0 & -1 & 0 & 1 & 0 & 0 & 0 & 0 & 0 & 0 \\ 0 & 0 & 0 & 0 & 0 & 0 & 0 & 1 & -1 & 0 \\ 0 & 0 & 0 & -1 & 0 & 0 & 0 & 1 & 0 & 0 \\ 0 & 0 & 0 & 0 & -1 & 0 & 0 & 1 & 0 & 0 \\ 0 & 0 & 0 & 0 & 0 & -1 & 0 & 1 & 0 & 0 \\ 0 & 0 & 0 & 0 & 0 & 0 & -1 & 1 & 0 & 0 \\ 1 & 0 & 0 & 0 & 0 & 0 & 0 & 0 & 0 & -1 \\ 1 & 0 & 0 & 0 & 0 & 0 & 0 & 0 & 0 & -1 \\ 1 & 0 & 0 & 0 & 0 & 0 & 0 & 0 & 0 & -1 \\ 1 & 0 & 0 & 0 & 0 & 0 & 0 & 0 & 0 & -1 \\ 1 & 0 & 0 & 0 & 0 & 0 & 0 & 0 & 0 & -1 \end{pmatrix}$$

and the propensity function is

$$\begin{aligned}\underline{a} = [&k_{\text{off}}^{\text{PLG}}x_2,\ k_{\text{on}}^{\text{PLG}}[\text{PLG}]^{\text{free}}x_3,\ k_{\text{off}}^{\text{PLi}}x_4,\ k_{\text{off}}^{\text{tPA}}x_4,\ k_{\text{on}}^{\text{PLG}}[\text{PLG}]^{\text{free}}x_5,\ k_{\text{off}}^{\text{PLG}}x_6,\ k_{\text{off}}^{\text{PLi}}x_7,\\ &k_{\text{off}}^{\text{tPA}}x_2,\ k_{\text{off}}^{\text{tPA}}x_3,\ k_{\text{off}}^{\text{PLi}}x_5,\ k_{\text{off}}^{\text{PLi}}x_6,\ k_{\text{cat}}^{\text{ap}}x_2,\ k_{\text{off}}^{\text{PLi}}x_9,\ k_{\text{deg}}x_4,\ k_{\text{deg}}x_5,\ k_{\text{deg}}x_6,\ k_{\text{deg}}x_7,\\ &k_{\text{cat}}^{n}nx_4,\ k_{\text{cat}}^{n}nx_5,\ k_{\text{cat}}^{n}nx_6,\ k_{\text{cat}}^{n}nx_7,\ k_{\text{cat}}^{n}nx_9],\end{aligned} \tag{A.2}$$

where n is the number of cryptic doublets at the binding location of interest. We use this information in the Gillespie Algorithm as follows:

(0) initialize $t = t_0$, $\underline{x} = \underline{x}_0$;

(1) with the system in state $\underline{x}$ at time t, evaluate the propensity function $\underline{a}$ and the sum $a_0(\underline{x}) = \sum_{j=1}^{22} a_j(\underline{x})$;

(2) choose two independent random variables, $r_1, r_2 \in U[0,1]$. Set $\tau = (1/a_0(\underline{x}))\ln(1/r_1)$ (when the next reaction happens) and set i to be the smallest integer such that $\sum_{j=1}^{i} a_j(\underline{x}) > r_2 a_0(\underline{x})$ (which reaction happens next);

(3) carry out reaction i and set $t = t + \tau$, $\underline{x} = \underline{x} + \underline{\nu}_i$.

A.2 *Quasi-steady state calculation for PLG*

The following is the quasi-steady state assumption calculation for plasminogen in the microscale model.

Assume that we have a system consisting solely of PLG and doublets (pairs of binding sites to which PLG can bind). Let p = free PLG concentration, N_{00}^j = concentration of N_{00} doublets of type j, N_{02}^j = concentration of N_{02} doublets of type j and N_{22}^j = concentration of N_{22} doublets of type j, where $j = i$ for intact, $j = n$ for nicked. Similarly, let k_{on}^j and k_{off}^j denote the rates for PLG binding to, and unbinding from, fibrin of type j. Then, we have the system of equations

$$\begin{aligned}\frac{\mathrm{d}N_{00}^i}{\mathrm{d}t} &= -2k_{\text{on}}^i pN_{00}^i + k_{\text{off}}^i N_{02}^i,\\ \frac{\mathrm{d}N_{02}^i}{\mathrm{d}t} &= -k_{\text{off}}^i N_{02}^i + 2k_{\text{on}}^i pN_{00}^i - k_{\text{on}}^i pN_{02}^i + 2k_{\text{off}}^i N_{22}^i,\\ \frac{\mathrm{d}N_{22}^i}{\mathrm{d}t} &= -2k_{\text{off}}^i N_{22}^i + k_{\text{on}}^i pN_{02}^i,\\ \frac{\mathrm{d}N_{00}^n}{\mathrm{d}t} &= -2k_{\text{on}}^n pN_{00}^n + k_{\text{off}}^n N_{02}^n,\\ \frac{\mathrm{d}N_{02}^n}{\mathrm{d}t} &= -k_{\text{off}}^n N_{02}^n + 2k_{\text{on}}^n pN_{00}^n - k_{\text{on}}^n pN_{02}^n + 2k_{\text{off}}^n N_{22}^n,\\ \frac{\mathrm{d}N_{22}^n}{\mathrm{d}t} &= -2k_{\text{off}}^n N_{22}^n + k_{\text{on}}^n pN_{02}^n.\end{aligned}$$

Making the quasi-steady state assumption, we set the right-hand sides of the above equations equal to zero. Let the total concentration of binding sites be F, so

$$F = \underbrace{N^i_{00} + N^i_{02} + N^i_{22}}_{F_i} + \underbrace{N^n_{00} + N^n_{02} + N^n_{22}}_{F_n}.$$

Then doing a bit of algebra gives the probability of having each type of doublet:

$$\begin{aligned}
P(N^i_{00}) &= \frac{0.5k^i_D F_i}{p\gamma_i(F_i+F_n)}, \quad P(N^n_{00}) = \frac{0.5k^n_D F_n}{p\gamma_n(F_i+F_n)},\\
P(N^i_{02}) &= \frac{F_i}{\gamma_i(F_i+F_n)}, \quad P(N^n_{02}) = \frac{F_n}{\gamma_n(F_i+F_n)},\\
P(N^i_{22}) &= \frac{0.5pF_i}{k^i_D\gamma_i(F_i+F_n)}, \quad P(N^n_{22}) = \frac{0.5pF_n}{k^n_D\gamma_n(F_i+F_n)},
\end{aligned}$$

where $\gamma_j = (1 + 0.5(k^j_D/p) + 0.5(p/k^j_D))$, $j = i$ or n. For $k^i_D = 38\,\mu\text{M}$, $k^n_D = 2.2\,\mu\text{M}$, $p = 2\,\mu\text{M}$,

$$\begin{aligned}
P(N^i_{00}) &= 0.9025\left(\frac{F_i}{F_i+F_n}\right), \quad P(N^n_{00}) = 0.2744\left(\frac{F_n}{F_i+F_n}\right),\\
P(N^i_{02}) &= 0.0950\left(\frac{F_i}{F_i+F_n}\right), \quad P(N^n_{02}) = 0.4989\left(\frac{F_n}{F_i+F_n}\right),\\
P(N^i_{22}) &= 0.0025\left(\frac{F_i}{F_i+F_n}\right), \quad P(N^n_{22}) = 0.2268\left(\frac{F_n}{F_i+F_n}\right).
\end{aligned}$$

In the model, we use these probabilities to determine where a plasmin molecule crawls. Once we know if the plasmin is moving onto a nicked or intact doublet, then we use the above probabilities without the $(F_i/(F_i+F_n))$ factor to determine if the given nicked or intact doublet is N_{00}, N_{02} or N_{22}.

A.3 *tPA rebinding probability*

Consider a molecule that can diffuse in a sphere of radius R_1 and bind to a partially absorbing inner sphere of radius $R_0 < R_1$. We think of R_0 as the size of the cross section of interest and R_1 as the distance to the next cross section. Let $\pi(r)$ be the probability of binding anywhere within the sphere of radius R_0 having started at radius r, so

$$D\frac{1}{r^2}\frac{\partial}{\partial r}\left(r^2\frac{\partial \pi}{\partial r}\right) - k_0\pi = -k_0, \quad \text{for } r \leqslant R_0, \tag{A.3}$$

and

$$D\frac{1}{r^2}\frac{\partial}{\partial r}\left(r^2\frac{\partial \pi}{\partial r}\right) = 0, \quad \text{for } R_0 < r \leqslant R_1, \tag{A.4}$$

where k_0 is the binding rate. Assuming that R_1 is an absorbing boundary gives the boundary condition $\pi(R_1) = 0$.

Solving for $\pi(R_0)$ gives the rebinding probability, i.e. the probably that a molecule starting at R_0 rebinds anywhere in the sphere of radius R_0:

$$\pi(R_0) = 1 - \frac{R_1}{R_0}\left(\frac{1}{1 + (R_1 - R_0)\sqrt{k_0/D}\coth(\sqrt{k_0/D}R_0)}\right), \tag{A.5}$$

where $D = 10^7$ nm^2/s (typical diffusion constant for an enzyme), $R_1 = 22.5$ nm (the distance to the next tPA binding site along the length of a fibrin fibre), $R_0 = 0.5$ nm (the assumed 'thickness' of the cross section) and $k_0 = k_{\text{tPA}}^{\text{on}} B$, where $k_{\text{tPA}}^{\text{on}}$ is the binding affinity of tPA to fibrin (in units of $1/\mu\text{M} \cdot \text{s}$) and B is the concentration of binding sites in the cross section (in units of μM).

When tPA unbinds from a doublet, we pick a random number. tPA rebinds if the random number is less than the rebinding probability, otherwise we conclude that the tPA molecule diffused away. The probability that a molecule will bind in the region $r \leqslant R_0$ is higher when there is a high concentration of binding sites and/or a strong binding affinity. The rebinding probability changes with time because B increases initially as binding sites are exposed and then decreases as degradation proceeds. However, for our parameters $\pi(R_0) = \mathcal{O}(10^{-6})$ and we conclude that tPA essentially never rebinds.

To derive equations (A.3), (A.4), consider the probability of a molecule being at position r_2, in state α_2 at time t_2 given that it started at position r_3, state α_3 at time t_3, $p(r_2, \alpha_2, t_2, r_3, \alpha_3, t_3)$. r_i is a continuous variable describing the physical location of the molecule and α_i is a discrete variable describing the state of the molecule. $\alpha_i = 0$ indicates the molecule is unbound and $\alpha_i = 1$ means the molecule is bound. When the molecule binds it remains bound, so

$$p(r_2, 1, t_2, r_3, 1, t_3) = 1, \tag{A.6}$$

$$p(r_2, 0, t_2, r_3, 1, t_3) = 0. \tag{A.7}$$

Let

$$P(r_2, t_2, r_3, t_3) = p(r_2, 0, t_2, r_3, 0, t_3),$$
$$Q(r_2, t_2, r_3, t_3) = p(r_2, 1, t_2, r_3, 0, t_3).$$

Since the molecule can diffuse and bind, P and Q satisfy the differential equations

$$\frac{\partial P}{\partial t_2}(r_2, t_2, r_3, t_3) = L_{r_2} P(r_2, t_2, r_3, t_3) - k_0 \chi(r_2) P(r_2, t_2, r_3, t_3), \tag{A.8}$$

$$\frac{\partial Q}{\partial t_2}(r_2, t_2, r_3, t_3) = k_0 \chi(r_2) P(r_2, t_2, r_3, t_3), \tag{A.9}$$

where L_{r_2} is the diffusion operator on r_2, k_0 is the binding rate and $\chi(r_2)$ is an indicator function such that

$$\chi(r_2) = \begin{cases} 1, & \text{if } r_2 \leqslant R_0, \\ 0, & \text{otherwise.} \end{cases}$$

Define $g(t_1, r_2) = \int Q(r_1, t_1, r_2, 0)\, dr_1$, the probability the molecule is bound at time t_1 given it started at position r_2 at time $t_2 = 0$. Then

$$\begin{aligned}\frac{\partial g}{\partial t_1} &= \int \frac{\partial}{\partial t_1} Q(r_1, t_1, r_2, 0)\, dr_1 \\ &= \int k_0 \chi(r_1) P(r_1, t_1, r_2, 0)\, dr_1 \qquad \text{(A.10)} \\ &= -\int_{t_1}^{\infty} \int \frac{\partial}{\partial t_1} k_0 \chi(r_1) P(r_1, t_1, r_2, 0)\, dr_1\, dt_1. \qquad \text{(A.11)}\end{aligned}$$

We show that

$$\frac{\partial}{\partial t_1} P(r_1, t_1, r_2, 0) = [L^*_{r_2} - k_0 \chi(r_2)] P(r_1, t_1, r_2, 0). \qquad \text{(A.12)}$$

Accepting this as true and using it in equation (A.11), we obtain

$$\begin{aligned}\frac{\partial g}{\partial t_1} &= -\int_{t_1}^{\infty} \int k_0 \chi(r_1)[L^*_{r_2} - k_0 \chi(r_2)] P(r_1, t_1, r_2, 0)\, dr_1\, dt_1 \\ &= -[L^*_{r_2} - k_0 \chi(r_2)] \int_{t_1}^{\infty} \left(\int \frac{\partial}{\partial t_1} Q(r_1, t_1, r_2, 0)\, dr_1 \right) dt_1 \\ &= [L^*_{r_2} - k_0 \chi(r_2)] \left(\int Q(r_1, t_1, r_2, 0)\, dr_1 - \int Q(r_1, \infty, r_2, 0)\, dr_1 \right). \qquad \text{(A.13)}\end{aligned}$$

Taking the limit of $\partial g / \partial t_1$ as $t_1 \to 0$ gives (via Equation (A.10)),

$$\begin{aligned}\lim_{t_1 \to 0} \frac{\partial g}{\partial t_1} &= \lim_{t_1 \to 0} \int k_0 \chi(r_1) P(r_1, t_1, r_2, 0)\, dr_1 \\ &= \int k_0 \chi(r_1) \delta(r_1 - r_2)\, dr_1 \\ &= k_0 \chi(r_2). \qquad \text{(A.14)}\end{aligned}$$

So Equation (A.13) becomes

$$k_0 \chi(r_2) = -[L^*_{r_2} - k_0 \chi(r_2)] \int Q(r_1, \infty, r_2, 0)\, dr_1. \qquad \text{(A.15)}$$

Let $\pi(r_2) = \int Q(r_1, \infty, r_2, 0)\, dr_1$, so

$$[L^*_{r_2} - k_0 \chi(r_2)] \pi(r_2) = -k_0 \chi(r_2). \qquad \text{(A.16)}$$

Equation (A.16) is equivalent to equations (A.3) and (A.4).

It remains to show equation (A.12). Because we have discrete and continuous variables, the Chapman–Kolmogorov equation is

$$p(r_1,\alpha_1,t_1,r_3,\alpha_3,t_3)=\sum_{\alpha_2=0,1}\int p(r_1,\alpha_1,t_1,r_2,\alpha_2,t_2)p(r_2,\alpha_2,t_2,r_3,\alpha_3,t_3)\,\mathrm{d}r_2, \tag{A.17}$$

where the function on the left-hand side is independent of t_2. Taking derivatives with respect to t_2 and dropping the terms that evaluate to 0 gives

$$\begin{aligned}
0&=\int\frac{\partial}{\partial t_2}p(r_1,0,t_1,r_2,0,t_2)p(r_2,0,t_2,r_3,0,t_3)\,\mathrm{d}r_2\\
&\quad+\int p(r_1,0,t_1,r_2,0,t_2)\frac{\partial}{\partial t_2}p(r_2,0,t_2,r_3,0,t_3)\,\mathrm{d}r_2\\
&=\int\frac{\partial}{\partial t_2}P(r_1,t_1,r_2,t_2)P(r_2,t_2,r_3,t_3)\,\mathrm{d}r_2\\
&\quad+\int P(r_1,t_1,r_2,t_2)\frac{\partial}{\partial t_2}P(r_2,t_2,r_3,t_3)\,\mathrm{d}r_2\\
&=\int\frac{\partial}{\partial t_2}P(r_1,t_1,r_2,t_2)P(r_2,t_2,r_3,t_3)\,\mathrm{d}r_2\\
&\quad+\int P(r_1,t_1,r_2,t_2)[L_{r_2}-k_0\chi(r_2)]P(r_2,t_2,r_3,t_3)\,\mathrm{d}r_2.
\end{aligned}$$

Integrating by parts yields

$$\begin{aligned}
0&=\int\frac{\partial}{\partial t_2}P(r_1,t_1,r_2,t_2)P(r_2,t_2,r_3,t_3)\,\mathrm{d}r_2\\
&\quad+\int P(r_2,t_2,r_3,t_3)[L^*_{r_2}-k_0\chi(r_2)]P(r_1,t_1,r_2,t_2)\,\mathrm{d}r_2,
\end{aligned} \tag{A.18}$$

where $L^*_{r_2}$ is the adjoint operator of L_{r_2}. Equation (A.18) simplifies to produce the adjoint equation

$$\frac{\partial}{\partial t_2}P(r_1,t_1,r_2,t_2)+[L^*_{r_2}-k_0\chi(r_2)]P(r_1,t_1,r_2,t_2)=0. \tag{A.19}$$

Because this is a time homogeneous process, $P(r_1,t_1,r_2,0)=P(r_1,0,r_2,-t_2)$ and

$$\frac{\partial}{\partial t_1}P(r_1,t_1,r_2,0)=-\frac{\partial}{\partial t_2}P(r_1,0,r_2,-t_2), \tag{A.20}$$

which with equation (A.19) gives

$$\frac{\partial}{\partial t_1}P(r_1,t_1,r_2,0)=[L^*_{r_2}-k_0\chi(r_2)]P(r_1,t_1,r_2,0).$$